Journal of Electron Spectroscopy and Related Phenomena 222 (2018) 149–155

Contents lists available at ScienceDirect

Journal of Electron Spectroscopy and Related Phenomena

journal homepage: www.elsevier.com/locate/elspec

Influence of spin–orbit coupling on the momentum distribution of electron pairs emitted from Au on Ir(111)

J. Kirschner[a,*], D. Vasilyev[a], F. Giebels[b], H. Gollisch[b], R. Feder[a,b]

[a] Max-Planck Institut für Mikrostrukturphysik, Weinberg 2, 06120 Halle, Germany
[b] Theoretische Festkörperphysik, Universität Duisburg-Essen, 47048 Duisburg, Germany

ARTICLE INFO

Article history:
Received 2 February 2017
Received in revised form 15 June 2017
Accepted 5 July 2017
Available online 14 July 2017

Keywords:
Surface physics
Spin-orbit coupling
Spin-split surface state
Spin-polarized electron scattering
Electron pair emission

ABSTRACT

We explore by theory and experiment the effects of spin–orbit coupling (SOC) on the pair creation of electrons by spin-polarized primary electrons incident on a pseudomorphic monolayer of Au on Ir(111). An ab-initio calculation of the electronic structure reveals a Rashba-type sp-like surface state in the Au layer, which turns out to lead to a large electron pair creation intensity. The distribution of this intensity over the momenta of the emitted electrons depends strongly on the primary electron spin due to spin–orbit coupling mainly in the incident and the outgoing electron states. For normal incidence, the six-fold rotation symmetry, which would hold without spin–orbit coupling, is broken in a manner depending on the orientation of the primary electron spin.

1. Introduction

The spin-dependence of electron-electron scattering in solids is generally brought about by spin–orbit and exchange interaction in the one-electron states as described by a Dirac equation with an effective magnetic field. For experimental studies two limiting cases are most useful: (a) scattering of polarized electrons from low-Z ferromagnets, which emphasizes the exchange interaction and (b) scattering of polarized electrons from high-Z non-magnetic solids, which singles out the spin–orbit interaction. The former case was harnessed a few years ago for a study of the exchange-correlation hole in the near-surface region of Fe(100) [1]. In the present paper we study the spin dependence of the electron pair intensity distribution due to electron scattering from a pseudomorphic monolayer of Au grown on Ir(111).

The basic idea is to send an electron of at a well-defined angle, energy and spin state on to a single-crystal surface of a sufficiently high-Z material in order to observe effects of spin–orbit coupling (SOC) in the scattering process. If the primary energy is high enough relative to the binding energy of a valence electron we may detect two electrons emitted from the surface. Hence the terminology (e,2e). We call the two electrons "a pair" because they are correlated with respect to their momenta, their total energy and their spin. The pair creation is experimentally studied by detecting the two electrons in coincidence on two detectors within a time window of a few nanoseconds. The spin dependence of this pair creation process is obtained by a second measurement where the primary electron spin is reversed. The resulting normalized difference of the pair creation rates gives rise to a "spin asymmetry". For comparison with experiment and for further analysis, spin-dependent (e,2e) rates were calculated by means of a relativistic multiple scattering formalism.

Experimental and theoretical (e,2e) results for Au on Ir(111) are presented in the form of distributions of the spin-averaged pair creation rate ("intensity") and of the difference between spin-up and spin-down rates ("intensity difference") over the momenta of the two emitted electrons ("momentum distributions"). In particular, we ask the following questions. (1) Can SOC substantially alter the symmetry of the momentum distributions? The answer is "yes" (see Section 5). (2) Can SOC significantly affect the extension of the exchange-correlation hole? The answer is "yes" or "no" depending on the primary electron energy (see Section 5).

2. Experiment

The experimental setup is shown schematically in Fig 1 . It consists of two channelplates and a spinpolarized electron source [2]. The photocathode is excited by light pulses from a diode laser [3] (pulse width of a few tenths of a nanosecond, repetition rate up to 20 MHz). At the exit of the gun we obtain a flux of single electrons which are sent to the target. The energy spectrum of the scattered

* Corresponding author.

https://doi.org/10.1016/j.elspec.2017.07.001
0368-2048/

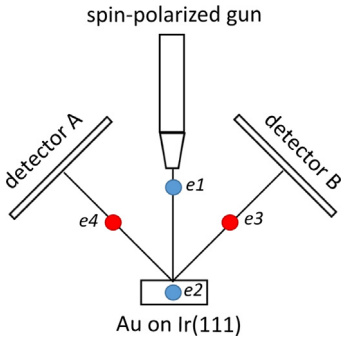

Fig. 1. Experimental setup (schematic) and labeling of the one-electron states. The spin polarization of the primary electrons is perpendicular to the paper plane.

electrons is determined by the time difference between the trigger to the light source and the electronic pulse from the anode of each of the channelplates. If the primary electron creates an electron pair the faster one opens a time window and the slower one closes it. If this happens we detect a coincidence event for a pair of electrons within this time window. We thus have a start pulse from the laser pulse trigger and two stop pulses. From this we calculate the electrons' flight times and from that the electrons' energies. The electronic signals are digitized by a fast digitizer [4] and analyzed by a PC running under LabView software.

Each of the channelplates is equipped with a double delay line [5]. The delay line signals are also digitized, triggered by the 'coincidence event' signal. From the delay line signals (difference and sum) we compute the location of each electron impact on the channelplate. These spatial informations are used (a) for a correction of the flight paths (shorter for an impact near the center of the anode and longer near its edge) and (b) for the determination of the angle at which an electron leaves the target surface. From this we determine the momentum of each electron within a pair. Overall we obtain a spatio-temporal resolution of typically 0.5 mm and 0.5 ns respectively for each coincidence event. The typical coincidence pair event rate is between one and ten per second.

As a sample we decided to use the pseudomorphic monolayer of Au on Ir because of some special properties: this system grows layer-by-layer, as first observed by Thomas in 1972 [6] and it is easy to produce a monolayer of Au on the surface. One first deposits a multilayer of Au on Ir by evaporation. The binding energy of Au on Au is lower than that of Au on Ir. Expressed in desorption temperature the Au desorption from Au occurs at 10° to 20 °K less than the desorption of Au from Ir (860 °C versus 880 °C). Therefore we apply a series of flashes at 860 °C until only a monolayer of Au remains [7]. The LEED pattern then is p(1 × 1) [8]. In the 10–10 mbar vacuum range this surface stays clean for more than 15 months. The adsorbed Au can be completely removed at about 1200 °C. A pseudomorphic Au monolayer is restored reliably by repeating the above procedure. A drawback of the high temperature flashes is that the crystal holder tends to creep slightly. After many cycles this creep came to rest at a crystal tilt angle of 4° (see below).

3. Theoretical methods

For the computation of spin-dependent (e,2e) momentum distributions from Au on Ir(001)we employed a formalism, which has been presented in detail in earlier work (c.f. [9,10]). We therefore only briefly recall its key features and formulae.

A primary electron with energy E_1, surface-parallel momentum component $\vec{k}_1^{\parallel}$ and spin orientation σ_1 relative to an axis $\vec{e}$ (i.e. spin polarization vector $\vec{P}_1 = \sigma_1 \vec{e}$ at the electron gun) collides with a valence electron with energy E_2, surface-parallel momentum component $\vec{k}_2^{\parallel}$ and spin label σ_2, and two outgoing electrons with $(E_3, \vec{k}_3^{\parallel}, \sigma_3)$ and $(E_4, \vec{k}_4^{\parallel}, \sigma_4)$ are detected. The four one-electron states $|E_i, \vec{k}_i^{\parallel}, \sigma_i\rangle$, in the following written as $|i\rangle$, with i=1,2,3,4 are solutions of the Dirac equation with a complex effective potential. The primary electron state $|1\rangle$ is a low-energy electron diffraction (LEED) state and the outgoing electron states $|3\rangle$ and $|4\rangle$ are time-reversed LEED states. While these states have definite spin orientation σ_i at the source and at the two detectors, respectively, inside the solid they involve parts with σ_i and parts with $-\sigma_i$ as a consequence of spin–orbit coupling. For the valence electron state $|2\rangle$, $\sigma_2 = \pm$ is in general only a label to characterize two degenerate states involving spin–orbit coupling. The initial two-particle state $|1, 2\rangle$ is an antisymmetrized product of states $|1\rangle$ and $|2\rangle$. The final two-electron state $|3, 4\rangle$ includes the Coulomb correlation between the one-electron states $|3\rangle$ and $|4\rangle$ (as described in detail in [10]).

For a spin-polarized primary beam impinging on a surface system, the spin-dependent (e,2e) scattering cross section ("intensity") is then given by the golden rule form

$$I^{\sigma_1}(E_1, \vec{k}_1^{\parallel}, E_3, \vec{k}_3^{\parallel}, E_4, \vec{k}_4^{\parallel}) = \frac{k_3 k_4}{k_1} \sum_{\sigma_3, \sigma_4} \sum_{E_2, \vec{k}_2^{\parallel}, \sigma_2, n_2} \left| \langle 3, 4|U|1, 2\rangle \right|^2 \delta, \tag{1}$$

where $k_i = \sqrt{2E_i}$ (for $i = 1, 3, 4$) and U is the screened Coulomb interaction. In the summation over the valence states $|2\rangle$ the index n_2 accounts for possible further degeneracies. δ symbolizes the conservation of energy and surface-parallel momentum

$$E_1 + E_2 = E_3 + E_4 \text{ and } \vec{k}_1^{\parallel} + \vec{k}_2^{\parallel} = \vec{k}_3^{\parallel} + \vec{k}_4^{\parallel} + \vec{g}^{\parallel}, \tag{2}$$

where $\vec{g}^{\parallel}$ is a surface reciprocal lattice vector. For fixed energies and parallel momenta of the primary electron and of the two detected electrons, one thus "picks out" valence electrons with definite energy and parallel momentum.

To perform numerical (e,2e) calculations for a specific surface system, the geometrical and the electronic structure of the ground state are required. To obtain these, we employed an ab-initio full-potential linear augmented-plane-wave (FLAPW) method [11], using a local density approximation (LDA) for the exchange-correlation energy [12]. Geometry and electronic densities of states results for Au/Ir(111) will be presented in Section 4. Further, the ab-initio calculation provided a real one-electron potential, which we used to construct the complex quasi-particle potential input for our (e,2e) calculations.

4. Geometrical and electronic structure

As described in Section 2, our surface system is a pseudomorphic monolayer of Au on Ir(111). The Au layer thus has the same surface-parallel unit cell as the Ir layers and the Au atoms are all within a single plane. To determine the spacing between the Au layer and the topmost Ir layer and the spacings between the near-surface Ir layers we resorted to an ab-initio calculation by the full-potential linearized augmented plane wave method with a local density approximation for the exchange-correlation energy [12] as implemented in the Juelich FLEUR computer code [11]. For a 31-layer film, which consists of 29 Ir layers and an Au monolayer on each side, we allowed the three topmost interlayer spacings to relax such that the total energy became minimal and the forces on the atoms were practically zero.

For the spacing between the Au layer and the topmost Ir layer we thus obtained 2.41 Å, which is larger than the interlayer spacing in bulk Ir (2.22 Å), and also larger than the interlayer spacing in bulk Au (2.36 Å) due to the lateral compression of the Au layer. The spacing between the first and second Ir layer is 2.15 Å and that between the second and third Ir layer is 2.19 Å, i.e. both are somewhat less than the bulk Ir spacing 2.22 Å.

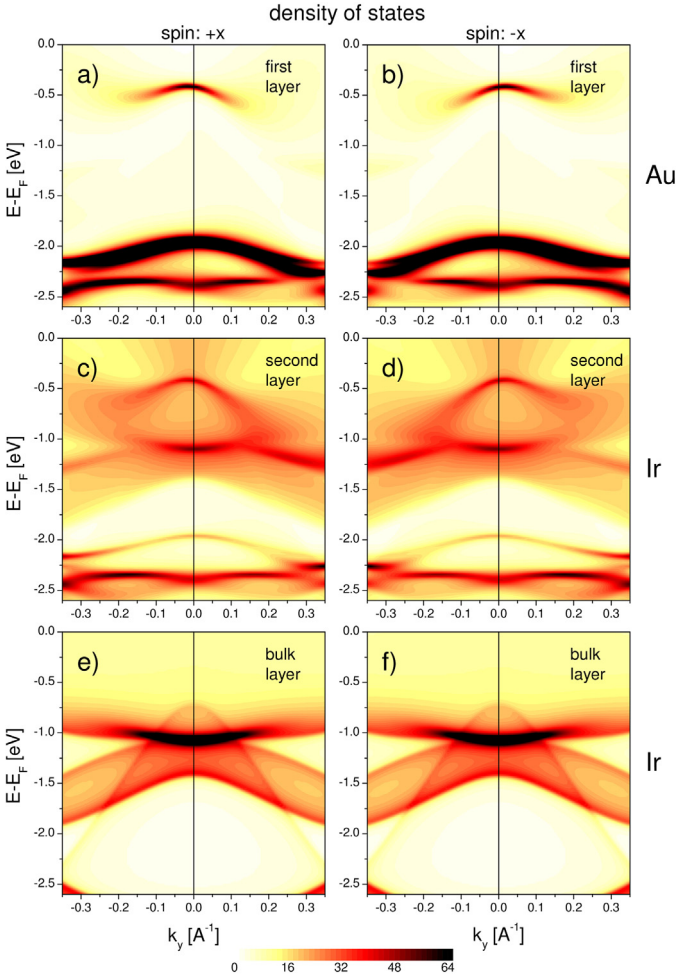

Fig. 2. Layer- and spin-resolved valence electron densities of states (LDOS) of 1ML Au/Ir(111) as functions of energy E and surface-parallel momentum (k_x=0, k_y) along the $\bar{K}-\bar{\Gamma}-\bar{K}$ line in the surface Brillouin zone. Surface coordinates x and y are along the [−1, −1, 2] and [1, −1, 0] directions, respectively. The spin orientation is along +x (left-hand column of panels) and −x (right-hand column of panels). The panels in the first, second and third row show the densities of states of the topmost layer (Au), the second layer (first Ir layer) and the bulk Ir layer, respectively.

Our ab-initio calculations for the 31-layer film with this geometry also yielded the electronic ground state structure. It is characterized in detail by the spin- and layer-resolved density of states (LDOS), which we present in Fig. 2 as function of energy and surface-parallel momentum (k_x = 0, k_y) along the $\bar{K}-\bar{\Gamma}-\bar{K}$ line in the surface Brillouin zone. This direction is chosen because in our (e,2e) geometry with off-normal incidence the momentum of the valence electron is along this line.

The bulk layers (Fig. 2 e and f) show Ir d-bands. In particular the high density of states at k_y = 0, i.e. the $\bar{\Gamma}$ point of the surface Brillouin zone, and 1 eV below the Fermi energy, corresponds to the L_{6-} point of the bulk band structure of Ir. The LDOS for spin up (Fig. 2e) and spin down (Fig. 2f) is the same, since the crystallographic inversion symmetry of Ir combined with time reversal symmetry implies spin degeneracy. At the surface, the inversion symmetry is broken and the LDOS in surface and near-surface layers becomes spin-dependent due to spin–orbit coupling. This phenomenon was first explored experimentally and theoretically on Au(111), which exhibits a spin-split sp-like surface state residing in a bulk L-gap near the Fermi energy (c.f. e.g. [13] and references therein), and is now commonly referred to as Rashba effect. For clean Ir(111), a spin-split surface state has been reported in ref. [14].

Turning now to the near-surface Ir layer of Au/Ir(111), panels c and d of Fig. 2 reveal two new structures, which are both spin-dependent. First we note an electronic state at −0.4 eV and k_y = 0, which disperses downward with k_y. This state resembles very closely the surface state on clean Ir(111) [14]. Second, a pair of bands appears below about −2 eV. Becoming much stronger in the Au layer (Fig. 2a and b), these bands are obviously Au-derived. We recall that the bulk Au d-band region is below about −2 eV.

The state found around −0.4 eV in the top Ir layer is seen to persist in the Au layer, with the same spin-dependent dispersion. Comparing with the surface state on clean Ir(111) [14], it becomes evident that this surface state is hardly affected by a monolayer of Au on Ir(111). Interestingly, it also survived a coverage by graphene [14].

The Ir-derived surface state on Au/Ir(111) is very advantageous as initial one-electron state for (e,2e) studies. First, it gives rise to a large reaction cross section. Second, due to its closeness to the Fermi energy there is hardly any inelastic multiple scattering, which would masque the genuine (e,2e) events.

5. Momentum distributions of electron pairs

In the following, we present experimental and theoretical (e,2e) results from Au/Ir(001). For fixed primary energy E_1 and surface-parallel momentum $\vec{k}_1^{\parallel}$, and outgoing electrons with fixed equal energy $E_3 = E_4$, it follows from energy and momentum conservation (Eq. (2)) that the spin-dependent intensities I^{σ_1} (c.f. Eq. (1)) are functions of the surface-parallel momenta $\vec{k}_3^{\parallel}$ and $\vec{k}_4^{\parallel}$ of the two outgoing electrons. Focusing on coplanar symmetric emission, we have $\vec{k}_4^{\parallel} = -\vec{k}_3^{\parallel}$ and the (e,2e) results can be presented as functions of $\vec{k}_3^{\parallel}$, which we refer to as momentum distributions.

Instead of the spin-dependent intensities I^+ and I^- (c.f. Eq. (1)), which differ from each other due to SOC, we show their sum and difference, since this makes the influence of SOC more visible. Our coordinate system is such that z is along the (outward-directed) surface normal [111], and x and y are in the surface plane along the [−1, −1, 2] and [1, −1, 0] directions, respectively.

Experimental and theoretical (e,2e) momentum distributions, which were obtained for primary electrons incident at polar angle 4° in the (y, z)-plane with energy 21 eV and spin orientation along y, are presented in Fig. 3. The reason for this particular angle has been described in Section 2. Conservation of parallel momentum then implies for a valence electron momentum $\vec{k}_2^{\parallel} = (k_{2x}, k_{2y}) = (0, 0.166\,\text{Å}^{-1})$. The choice $E_3 = E_4$ = 7.45 eV together with the work function of 5.7 eV (obtained from our ab initio calculations) sets the valence electron energy at 0.4 eV below the Fermi energy. For the experimental intensity distributions in Fig. 3 we have set an energy window of about 1 eV width, centered around −0.5 eV below the Fermi level. Thus, they are related to the arc-like structures in the LDOS of Fig. 2 near $\vec{k}_2^{\parallel} = 0$, derived from the Au states (Fig. 2a and b) and the hybridized Au-Ir states in the second layer (Fig. 2c and d). In the intensity distributions in Fig 3 we find a maximum in the second quadrant (k_x = 0 to −1 Å^{-1}, k_y = 0 to 1 Å^{-1}) and a second maximum in the fourth quadrant (k_x = 0 to 1 Å^{-1}, k_y = 0 to −1 Å^{-1}). For the intensity differences we observe predominantly positive (negative) values in the second (first) and fourth (third) quadrant. Although the experimental data are somewhat blurred by the counting statistics we clearly see a twofold rotation symmetry in experiment and theory. Disregarding the details we state a satisfactory agreement of the intensities and the spin-related results.

Because of the off-normal incidence, the entire setup no longer has the threefold rotation symmetry about the surface normal. There is however another symmetry property. Since for equal energies $E_3 = E_4$ and coplanar symmetric emission the results are invariant against interchanging the two detection directions deter-

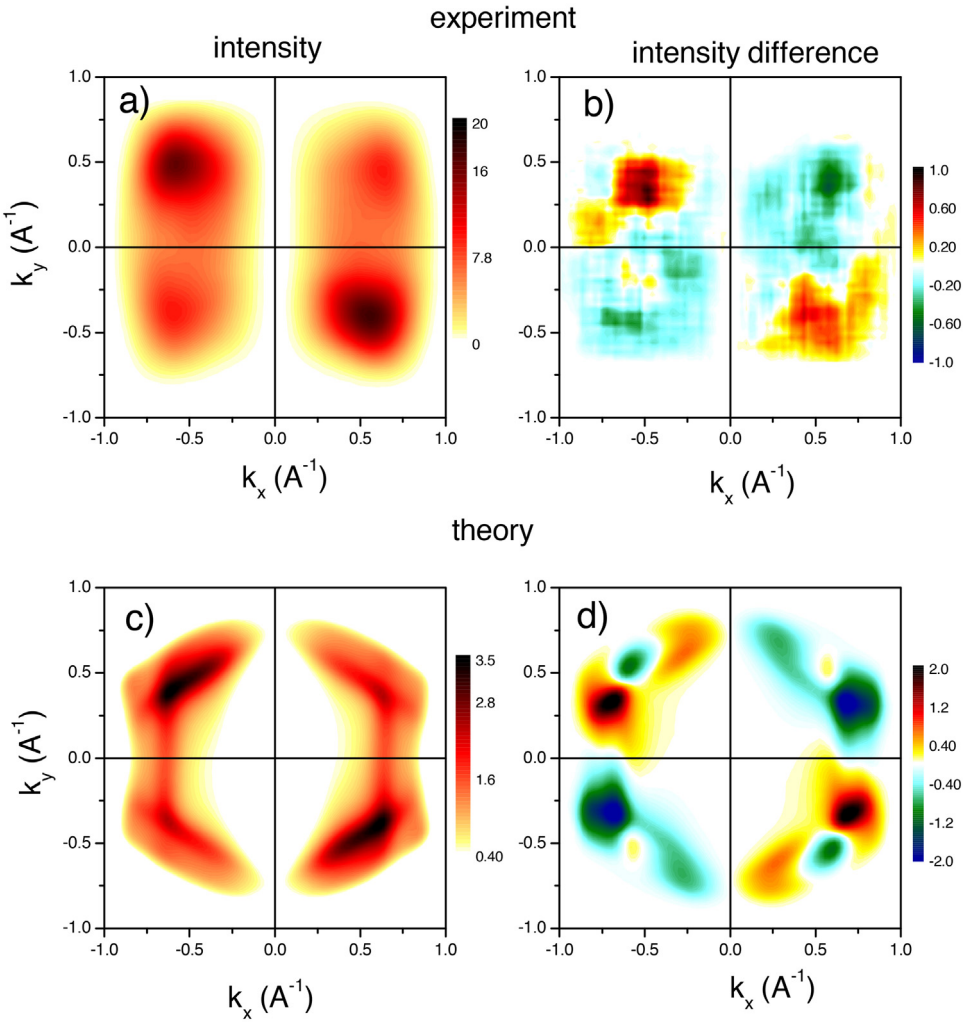

Fig. 3. (e,2e) momentum distributions from Au/Ir(111) in the surface-parallel momentum plane (k_x, k_y) with k_x and k_y along the $\bar{M} - \bar{\Gamma} - \bar{M}$ and $\bar{K} - \bar{\Gamma} - \bar{K}$ lines in the Surface Brillouin Zone, respectively. Primary electrons with energy 21 eV are incident in the (y, z)-plane at polar angle $\vartheta_1 = 4°$. They are spin-polarized along $\pm y$, producing (e,2e) intensities I^+ and I^-. Panels a and b show the measured intensity sum $I^+ + I^-$ and intensity difference $I^+ - I^-$ (with positive/negative values for spin up/down), respectively, in units of event counts divided by 1000. Their theoretical counterparts are presented in panels c and d (in arbirary units).

mined by $\vec{k}_3^{\parallel}$ and $\vec{k}_4^{\parallel}$, the momentum distributions should exhibit two-fold rotation symmetry about the axis normal to the momentum plane. This is seen to be exactly so in the theoretical results (Fig. 3c and d) and approximately so in the experimental ones (Fig. 3a and b).

While the results in Fig. 3 are restricted in momentum space according to the size and position of the detector channel plates, we show in Fig. 4 complete theoretical results up to the maximal $\vec{k}_3^{\parallel}$ values determined as $|\vec{k}_3^{\parallel}| = \sqrt{2E_3}$. The total intensity in Fig. 4a and the intensity difference in Fig. 4b are obviously extensions of the results in Fig. 3c and d, both clearly exhibiting the two-fold rotation symmetry. Changing the primary spin orientation from y to x, the total intensity remains the same, but the intensity difference (shown in Fig. 4c) is – while comparable in size and still two-fold symmetric – distributed in strong contrast to the one in Fig. 4b.

The results presented so far were obtained for off-normal incidence with $\vartheta_1 = 4°$. We now turn to the case of normal incidence, which in particular reveals the effect of SOC on symmetry properties. We first note that according to Eq. (2) $\vec{k}_1^{\parallel} = 0$ dictates $\vec{k}_2^{\parallel} = 0$, i.e. the relevant valence electrons are at the center of the SBZ. With outgoing energies chosen such that the valence energy is 0.4 eV below the Fermi energy, the densities of states in Fig. 2a show that we are dealing with the pronounced sp-like surface state.

In Fig. 4d the distribution of the total intensity, i.e. the sum $I^+ + I^-$ (c.f. Eq. (1)), which is obtainable by using an unpolarized primary beam, is seen to exhibit six-fold rotation symmetry about the surface normal. This is due to the threefold rotation symmetry of the crystal combined with the two-fold rotation symmetry due to invariance against interchanging the two detection directions. In contrast, the symmetry of the intensity difference $I^+ - I^-$ is reduced due to SOC in a manner dependent on the primary spin orientation σ_1.

For σ_1 along y, the distribution (in Fig. 4e) no longer has six-fold rotation symmetry, but only a two-fold one plus a mirror symmetry with respect to the (x, z)- and one to the (yz) plane normal to the surface. These two mirror symmetries are easily understood as follows. We first note that the (x, z)-plane is a mirror plane of the crystal. Since the primary spin along y is normal to this plane, it is invariant against reflection at this plane and so are consequently the intensity difference distributions. Combining this mirror symmetry with the two-fold rotation symmetry entails mirror symmetry with respect to the (y, z)-plane.

If the primary spin σ_1 is along x, it is reversed by reflection at the (x, z) plane. Consequently, this reflection must reverse the sign of the intensity difference. Combined with the two-fold rotation symmetry, a sign reversal also occurs by reflection at the (y, z) plane.

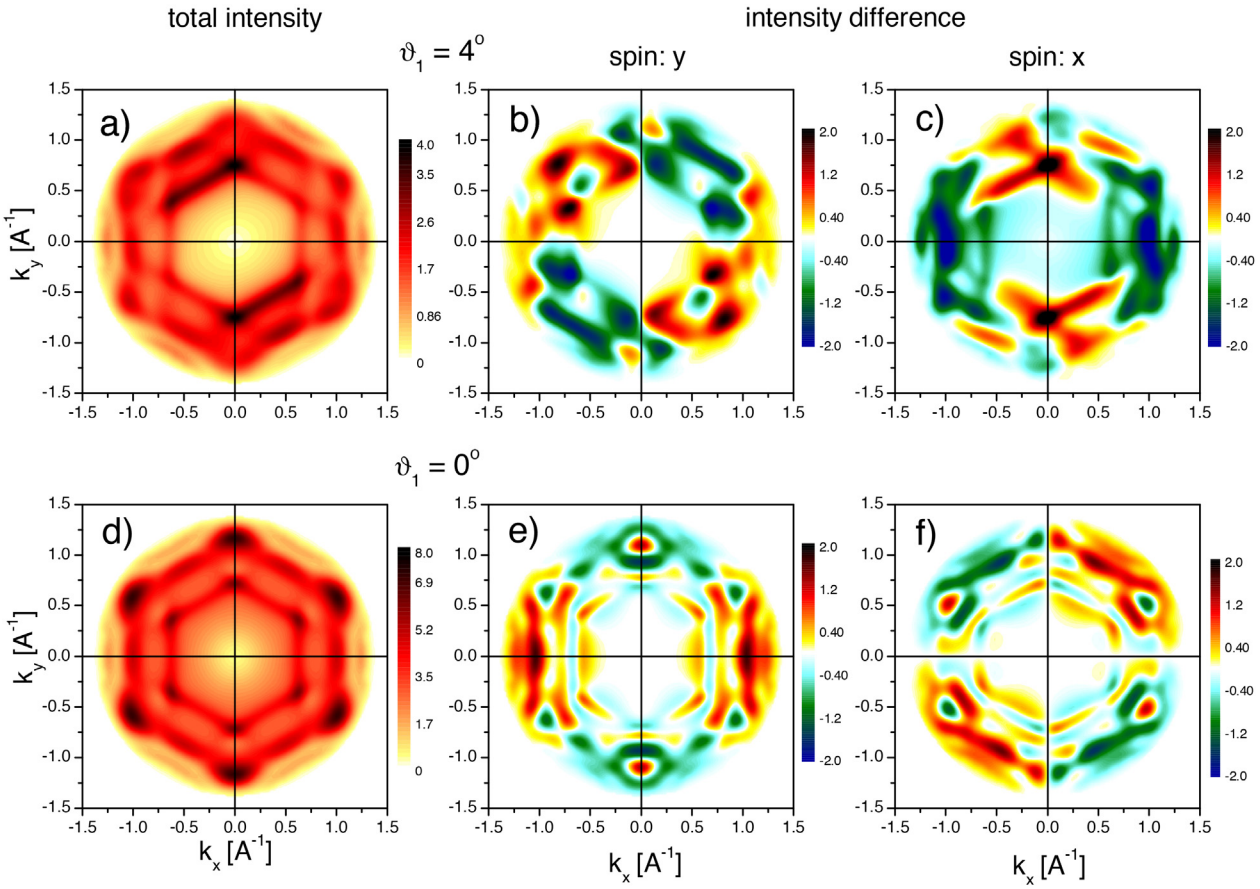

Fig. 4. Calculated (e,2e) momentum distributions from Au/Ir(111) in the surface-parallel momentum plane (k_x, k_y) with k_x and k_y along the $\bar{M} - \bar{\Gamma} - \bar{M}$ and $\bar{K} - \bar{\Gamma} - \bar{K}$ lines in the Surface Brillouin Zone, respectively. For primary electrons with energy 21 eV incident at polar angle $\vartheta_1 = 4^\circ$ in the (y, z)-plane, the intensity sum is presented in panel a. Panels b and c show the intensity difference for primary spin orientation $\pm y$ and $\pm x$, respectively. Analogous results obtained for normal electron incidence are presented in panels d, e and f. The results in all the panels are in the same arbitrary units.

These properties are illustrated quantitatively in Fig. 4f. Comparison of panels e and f of Fig. 4 demonstrates that the distribution of the intensity difference depends strongly on the orientation of the primary electron spin.

The above intensity distributions were obtained with SOC present in each of the four one-electron states. In order to find out which of these states might be most responsible for producing the observed SOC effects, we performed further calculations, in which SOC was selectively switched off in one or more of the states. Results are presented in Fig. 5. Looking first at the (spin-averaged) total intensity in the left-hand column, it is seen to decrease from the all-SOC distribution (Fig. 5a) in a comparable way if SOC is switched off either for the two outgoing electrons (Fig. 5c) or for the primary electron (Fig. 5e). The central region of the distribution weakens further for SOC switched off for primary and outgoing electrons (Fig. 5g). It thus appears that SOC leads to an enhancement of the (e,2e) reaction cross section, in particular in the central region, i.e. to a reduction of the exchange-correlation hole. Further calculations for different primary energies revealed however, that this is not so in general. As an example, we show in Fig. 6 analogous results obtained for primary energy 17 eV. The intensity distribution with SOC in all states (Fig. 6a) is seen to be almost the same as the one with SOC switched off for primary and outgoing electrons (Fig. 6g). Such different behaviour for different primary energies is plausible, since different LEED-type states enter into the Coulomb matrix elements, which determine the (e,2e) cross section (c.f. Eq. (1)).

The effects of selectively switching of SOC on the intensity difference distributions, which owe their very existence to SOC, is illustrated in the right-hand columns of Figs. 5 and 6. For primary energy 21 eV, the all-SOC distribution (Fig. 5b) differs only rather moderately from the one with SOC switched off for the outgoing electrons (Fig. 5d). Switching off SOC for the primary electron (Fig. 5f) produces similar changes, but with the sign in several regions reversed. If SOC is absent in all three LEED-type states (Fig. 5h), very little remains. If SOC is switched off in all four states, the intensity difference is of course identically zero. For primary energy 17 eV, the intensity difference distributions are seen to respond to switching off SOC in a similar way (see Fig. 6).

6. Conclusion

The electronic structure of a pseudomorphic monolayer of Au on Ir(111) exhibits a Rashba-like surface state, which gives rise to a large (e,2e) reaction cross section. Together with the large Z of Au and Ir, this makes Au on Ir very suitable for studying the influence of spin–orbit coupling (SOC) on (e,2e). Using spin-polarized primary electrons, we measured and calculated spin-dependent (e,2e) intensities. The results were presented in the form of momentum distributions of the spin-averaged intensity and of the difference between the spin-up and spin-down intensities. Experimental momentum distributions turned out to agree rather well with their theoretical counterparts.

The observed intensity differences are sizeable, and their momentum distributions are richly structured with distinct symmetry properties. For normal incidence of the primary electron, the symmetry is of type 2mm, i.e. a two-fold rotation axis and two per-

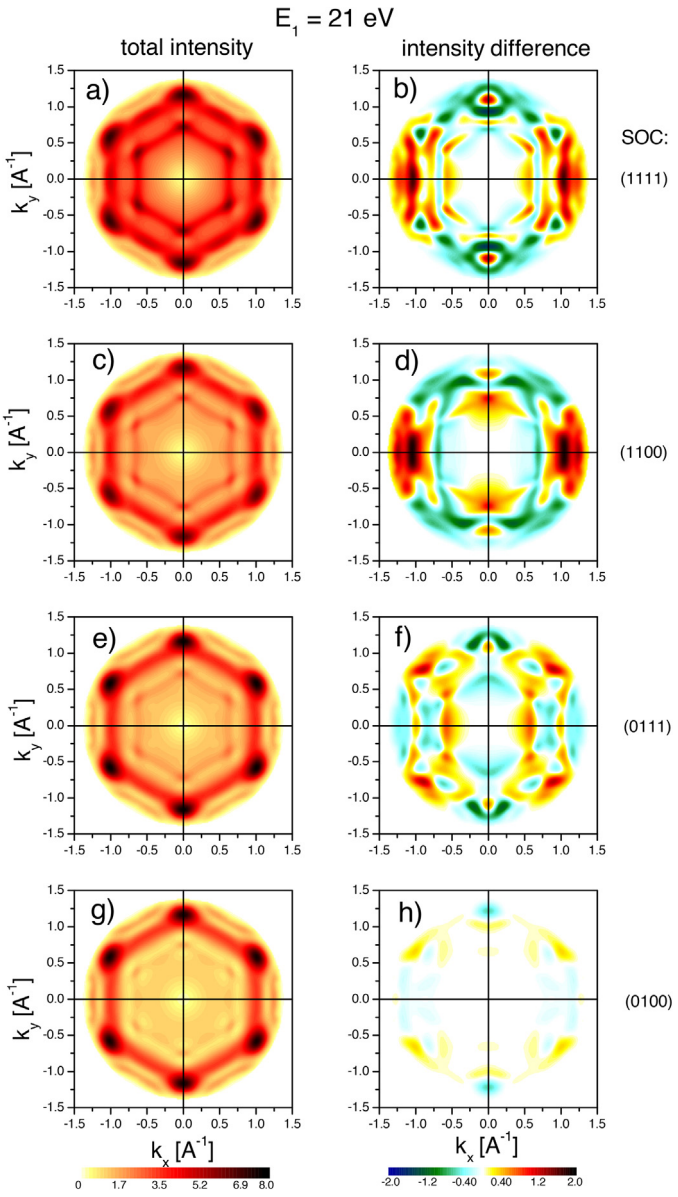

Fig. 5. Calculated (e,2e) momentum distributions from Au/Ir(111) of intensity sum and of intensity difference for normally incident primary electrons with energy 21 eV and spin along $\pm y$. While the results in panels a and b were obtained with SOC taken into account completely, i.e. in all four one-electron states (1 primary electron, 2 valence electron, 3 and 4 outgoing electrons) the subsequent rows of panel demonstrate the effect of switching off SOC selectively in these states. The notation (nnnn) on the right-hand side of each row indicates in which of the one-electron states SOC has been taken into account ($n = 1$) or neglected ($n = 0$). Thus e.g. (1100) in the second row of panels means that SOC was taken into account in states 1 and 2, whereas it was switched off in states 3 and 4. Results for (0000), i.e. SOC absent in all four one-electron states, are not shown since in this case the intensity difference is identically zero.

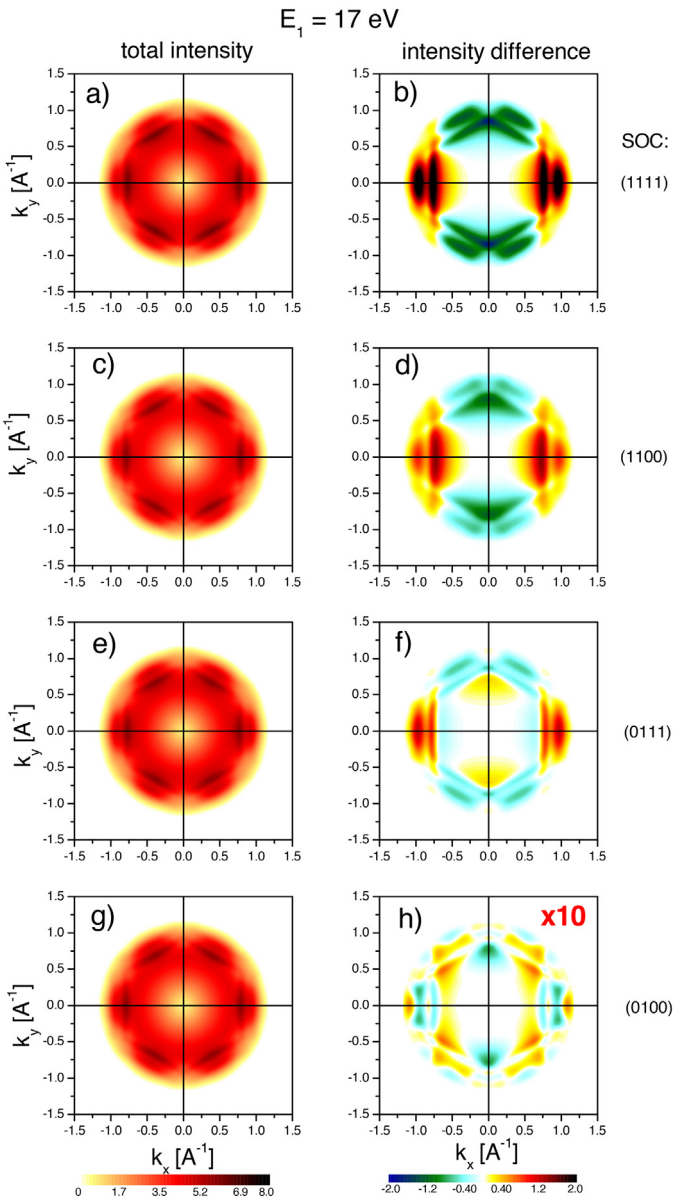

Fig. 6. As Fig. 5, but for primary electron energy 17 eV. Note that panel h shows the intensity difference multiplied by a factor 10.

pendicular mirror planes. This is in contrast to the 6-fold rotation symmetry of the distribution of the spin-averaged intensity and of the intensity calculated without SOC. The symmetry of the momentum distributions is thus substantially altered by SOC. This effect is independent of the primary electron energy.

In contrast, the influence of SOC on the extension of the exchange-correlation hole, the central depletion zone in the momentum distributions, was found to depend on the primary energy. For example, for primary energy 24 eV the extension of the hole is significantly reduced by SOC, whereas for 17 eV it is practically unaffected. Such dependence on primary energy is due to the fact that the Coulomb matrix elements (c.f. Eq. (1)) comprise quite different LEED-type states (representing primary and outgoing electrons).

References

[1] F. Giebels, H. Gollisch, R. Feder, F.O. Schumann, C. Winkler, J. Kirschner, Spin-dependent two-electron emission from ferromagnetic Fe(001), Phys. Rev. B 84 (2011) 165421.
[2] Yu.A. Mamaev, L. G: Gerchikov, Yu.P. Yashin, D.A. Vasilyev, V.V. Kuzmichev, V.M. Ustinov, A.E. Zhukov, V.S. Mikhrin, A.P. Vasiliev, Optimized photocathode for spin-polarized electron sources, Appl. Phys. Lett. 93 (2008) 081114.
[3] PicoQuant, www.picoquant.com, Series LDH.
[4] Acquiris digitizer type DC 282, resolution 0.5 nsec.
[5] Roentdek, www.roentdek.com, type DLD.
[6] R.E. Thomas, Interference effects in the reflection of low-energy electrons from thin films of Au on Ir, J. Appl. Phys. 41 (1970) 5530.
[7] D. Vasilyev, C. Tusche, F. Giebels, H. Gollisch, R. Feder, J. Kirschner, Low-energy electron reflection from Au-passivated Ir(001) for application in imaging spin-filters, J. Electr. Spectros. Relat. Phenom. 199 (2015) 10, This was first observed for Ir(100), and it was observed also for Ir(111).
[8] S. Ogura, K. Fukutani, M. Okada, Structure of gold thin films grown on Ir(111), Top. Catal. 44 (2007) 65.

[9] R. Feder, H. Gollisch, in: W. Schattke, M.A. Van Hove (Eds.), Low-Energy (e,2e) Spectroscopy, Solid State Photoemission and Related Methods, Wiley-VCH, Weinheim, 2003.
[10] H. Gollisch, N.v. Schwartzenberg, R. Feder, Emission of correlated electron pairs from solid surfaces, Phys. Rev. B 74 (2006) 075407.
[11] See www.flapw.de.
[12] S.H. Vosko, L. Wilk, M. Nusair, Accurate spin-dependent electron liquid correlation energies for local spin density calculations: a critical analysis, Can. J. Phys. 58 (1980) 1200.
[13] J. Henk, M. Hoesch, J. Osterwalder, A. Ernst, P. Bruno, Spin–orbit coupling in the L-gap surface states of Au(111): spin-resolved photoemission experiments and first-principles calculations, J. Phys.: Condens. Matter 16 (2004) 7581.
[14] A. Varykhalov, D. Marchenko, M.R. Scholz, E.D.L. Rienks, T.K. Kim, G. Bihlmayer, J. Sanchez-Barriga, O. Rader, Ir(111) surface state with giant Rashba splitting persists under graphene in air, Phys. Rev. Lett. 108 (2012) 066804.